Research Article | Vol. 28, No. 9 / 27 April 2020 / Optics Express 13131
Optics EXPRESS

Beam waist shrinkage of high-power broad-area diode lasers by mode tailoring

JIAXIN SU,[1,2] CUNZHU TONG,[1,*] LIJIE WANG,[1] YANJING WANG,[1,2] HUANYU LU,[1,2] ZHIDE ZHAO,[3] JUN WANG,[3] SHAOYANG TAN,[3] SHILI SHU,[1] AND LIJUN WANG[1]

[1]*State Key Laboratory of Luminescence and Applications, Changchun Institute of Optics, Fine Mechanics and Physics, Chinese Academy of Sciences, Changchun 130033, China*
[2]*Center of Materials Science and Optoelectronics Engineering, University of Chinese Academy of Sciences, Beijing 100049, China*
[3]*Suzhou Everbright Photonics Co., Ltd, Suzhou 215000, China*
[*]*tongcz@ciomp.ac.cn*

Abstract: A new approach was proposed and its role in improvement of the beam quality of high-power broad-area diode lasers was demonstrated, in which a composite arrow array and trench microstructure was used to suppress the beam waist and tailor the high order lateral modes. The beam waist shows a special shrinkage with increasing injection current resulting from the combined effect of mode tailoring and the thermal lens effect. A 58% improvement in lateral beam parameter product was realized compared with conventional broad-area diode lasers.

1. Introduction

High-power diode laser systems based on broad-area (BA) diode lasers are well established laser sources for a variety of applications [1–5], including industrial material processing, medical treatment, display technology and pumping solid-state lasers or fiber lasers. The main advantages of such systems are high power conversion efficiency, high optical power, reliability, long lifetime, relatively low cost, small size and mature technology. However, BA diode lasers are limited for use in further applications by the poor beam quality and low brightness. Progress on the beam quality of BA lasers will have significant potential effects on the development of high-power diode lasers and fiber lasers.

The poor far-field performance of high-power BA lasers includes high divergence in the slow-axis and the coherence of the injected current, also called as far-field blooming [6]. The intrinsic reason is the allowance of multiple lateral modes and the thermal effect. Although the broadened waveguide increases the volume of the gain medium and heat dissipation channel and hence realizes impressive power, operation of multiple lateral modes deteriorates the beam quality in the lateral direction (slow axis). To improve the beam quality, numerous methods have been proposed to reduce the divergence angle of BA lasers in the lateral direction of waveguide, including a modal reflector at the facet [7], resonant anti-guiding [8], a spatial phase controller [9,10], filtering microstructure [11,12], and an angled waveguide [13]. Actually, the beam quality of a laser beam is characterized by the product of the beam divergence and the beam waist at the focus point. This means that improvement of beam quality can also be achieved from the point of view of the beam waist. Generally speaking, it is more difficult to realize a decreased beam waist with increasing current for BA lasers than to realize a decrease in beam divergence. Hence, few investigations have focused on control of the beam waist.

In this paper, a new approach to realize beam waist shrinkage and to suppress far-field blooming is proposed. The approach is based on a symmetric arrow-array structure located near the facets of BA lasers, and two long and narrow trenches along the cavity. The arrow arrays play the role of tailoring the lateral modes and hence decreases the beam waist. Two trenches are used to

#390265 https://doi.org/10.1364/OE.390265
Journal © 2020 Received 11 Feb 2020; revised 31 Mar 2020; accepted 3 Apr 2020; published 17 Apr 2020

Optics EXPRESS

weaken the lateral carrier accumulation (LCA) effect and provide mode filtering. Related models were established to explain the decrease in the far field angle and beam waist shrinkage, which may be caused by the positive thermal lens effect. The influence of this composite microstructure on the light-injected current-voltage (L–I–V) performance, near-field, far-field and beam quality was measured and analyzed.

2. Device design and simulation

The beam quality of a BA diode laser can be described by the beam parameter product (BPP) and the M^2 factor, which have only a factor difference of π/λ. The BPP is defined as the product of beam waist and divergence, i.e., BPP = $w_{95\%}\theta_{95\%}/4$, where $w_{95\%}$ and $\theta_{95\%}$ are respectively the diameter of the beam waist and far-field divergence for 95% power content. A small BPP value is desired for high power diode lasers. However, the BPP values of high-power BA diode lasers often suffer from a widening in the lateral direction with increasing current. The main reason originates in self-heating and the LCA [14]. The former is hard to avoid and generates a lateral thermal lens in the active region. The LCA occurs because of the diffusion of carriers in the lateral direction of a BA waveguide and their accumulation at the edge of the waveguide, which promotes the lasing of high-order lateral modes; hence, slow-axis far-field blooming [7] occurs.

Our previous works [15–17] demonstrated that deeply etched trenches were able to suppress the LCA, and the mode tailoring microstructure [12,18] could control the high-order lateral modes. Therefore, we designed a composite microstructure that consists of a strong mode tailoring microstructure and trenches to combine these two effects. Figure 1(a) shows a schematic of the proposed composite microstructure. The mode tailoring was realized by four groups of arrows on each corner of the BA waveguide surface; two long trenches were used to suppress the LCA. To simplify, this composite microstructure is called the arrow-trench (AT) microstructure. The designed period of the arrows is 25 μm. The length of the trenches is 1440 μm and the width is 3 μm. The distance between two AT microstructures, d, is 55 μm. Figure 1(b) shows the cross-section of the waveguide. The ridge width L is 100 μm, and the cavity length is 1500 μm, with an etching depth of 1.2 μm. The light suffers less loss and the mode selection scale is adjusted at this depth, based on our previous fabrication experiments. The separation between the two trenches from center to center was 91 μm. The detailed arrow microstructure is shown in Fig. 1(c); the structure parameter a is 70°, b is 15 μm and c is 4 μm.

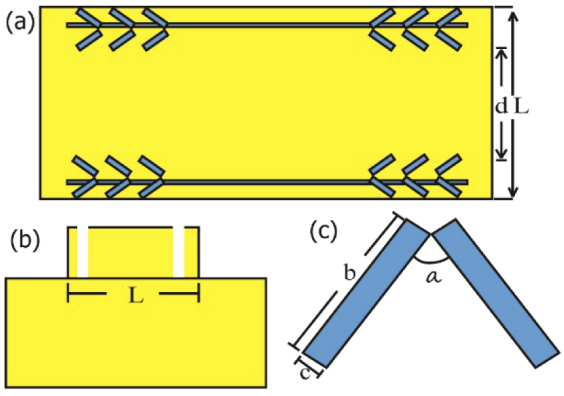

Fig. 1. Schematic of AT laser: (a) top view, (b) cross-section, and (c) detail of arrow pattern.

To verify the role of the proposed AT structure in controlling the lateral modes, simulation using the two-dimensional finite difference time domain (FDTD) method was performed. The

Optics EXPRESS

facet area of a BA laser with arrow arrays and two trenches was selected. The whole area was 130 μm long and 110 μm wide. Figure 2(a) shows the optical field distribution after passing through the AT microstructure for mode order m=4. The BA laser without this microstructure is denoted the standard BA laser. Compared with the standard BA laser, the AT laser shows obvious beam waist shrinkage, from five peaks down to three peaks. Figures 2(b)–2(f) show the calculated optical field distribution of lateral modes through the AT microstructure area with mode orders of m=0, 1, 2, 5 and 9, respectively. It can be clearly seen that the arrow arrays and the trenches give an evident double reflection, which causes the light scattering near the edges and an increased optical path at the edge; hence, the energy distribution is changed and high-order lateral modes are suppressed. Figure 3 shows a comparison of the energy distribution of the different modes after passing through the AT microstructure. This microstructure changed the distribution of every mode and centralized them, and the selectivity of different lateral modes was changed. In this way, the beam waists may shrink toward the center of the ridge waveguide.

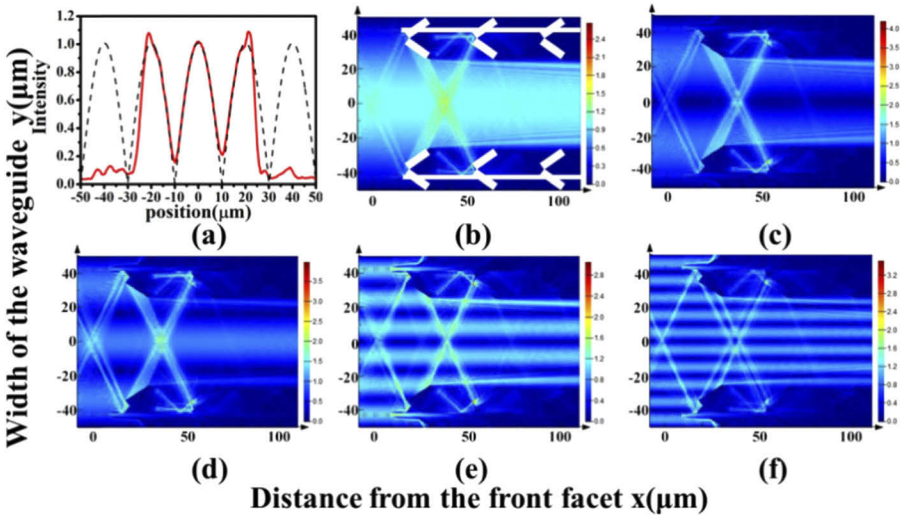

Fig. 2. (a) Calculated optical field distribution at the facet of BA laser without (black) and with (red) AT microstructure for mode m=4, (b) to (f) are the optical field distributions of lateral modes with order numbers m=0, 1, 2, 5 and 9 through the AT microstructure, respectively.

Obviously, the AT microstructure tailors almost all the modes, which is not expected for high-power high beam quality. To retain more of the fundamental order mode, the size of the AT microstructure was optimized. Figure 4 shows the ratio R_u of the integrated optical-field intensity retained after passing through the AT structure as a function of (L-d)/L, where L is the width of the ridge waveguide and d is the width of the center area remaining. Here, L is 100 μm. (L-d) represents the size of the AT microstructure, and an increase in the value of (L-d) means only that the value of b shown in Fig. 1(c) increases. The R_u of all the modes decrease with an increase in the size of the AT microstructure, and the fundamental mode suffers less energy loss than that of high-order modes. The intensity of the fundamental mode is approximately 1.5 times higher than the other modes at (L-d)/L ratios of 0.4 to 0.5. Therefore, a tailoring ratio of 0.45 was chosen in the following experiment to increase the loss difference between the fundamental mode and high-order modes, resulting in decreased lateral divergence.

Optics EXPRESS

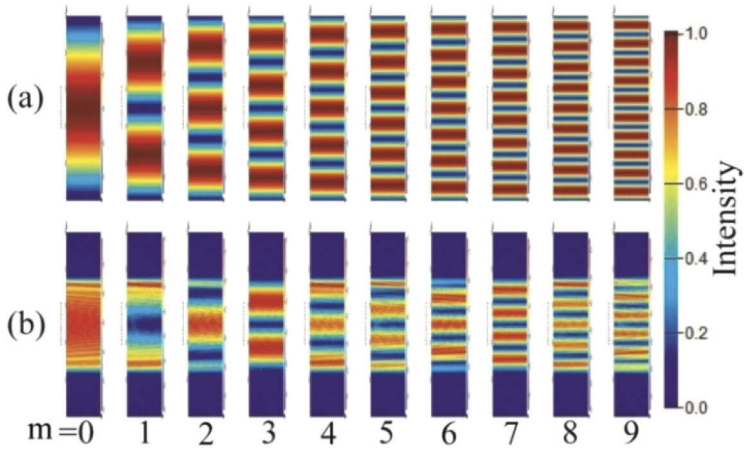

Fig. 3. Calculated near-field of (a) standard BA lasers and (b) BA lasers with AT microstructure. The lateral mode orders are m=0 to 9.

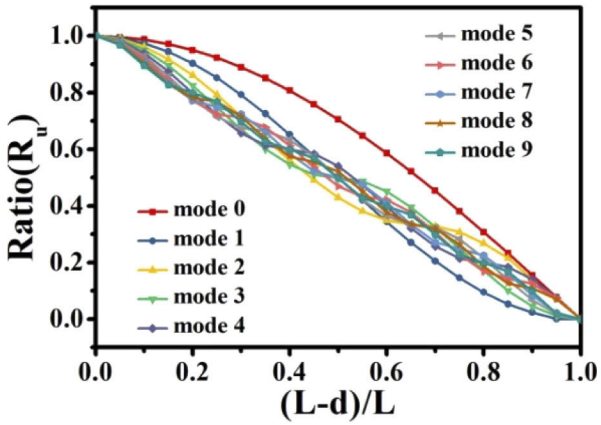

Fig. 4. Energy retained after transmitting different modes through the microstructure.

3. Experiment

The epitaxial structure of the laser devices was a typical asymmetric super-large optical cavity (SLOC) and was grown by metal organic chemical vapor deposition (MOCVD) on an (001)-oriented 3-in n+ GaAs substrate. The SLOC consisted of 3.0-μm and 1.2-μm n- and p-type doped AlGaAs waveguides, respectively. The gain material was two InGaAs quantum wells (QWs) with an emission wavelength of 925 nm. After the MOCVD growth, a 100-μm-wide-ridge and AT microstructures were fabricated by inductively coupled plasma (ICP) etching. The etch depth was 1.2 μm down to the p-type waveguide layer. The AT lasers and standard BA lasers were manufactured on the same wafer using the same lithograph mask for comparison. After that, an insulation layer of 200-nm-thick SiO_2 was deposited at 300 °C by plasma-enhanced chemical vapor deposition (PECVD). The contact window was formed by reactive ion etching (RIE), after which ohmic contacts were fabricated on the top and back of the wafer by magnetron sputtering. The p-type and n-type contact metals were respectively Ti-Pt-Au and Au-Ge-Ni-Au. After annealing to achieve low contact resistance, the wafer was cleaved into individual devices.

Optics EXPRESS

The devices were mounted on a copper heatsink with the p-side down without facet passivation or coating for testing.

4. Results and discussion

4.1. L–I–V characteristics

Figure 5 shows the L–I–V characteristics of the standard laser and the AT laser under continuous wave (CW) operation at room temperature. The output power of the standard laser at 4 A is 1.743 W (single facet); with the same injection current, the output power of the AT laser is 2.117 W (single facet), approximately 21% higher than that of the standard laser. The highest power conversion efficiencies (PCE) (both facets) of these two types of devices are 48.5% for standard lasers and 55.2% for the AT laser. The voltage of the AT laser is higher than that of the standard laser, which may be caused by higher resistivity resulting from the microstructures and the trenches. The AT laser shows higher output power and lower threshold current than the standard laser, the reason might be the suppressed LCA effect due to the deep etched trenches improves the matching between the mode profile and injected current profile, which will increase the modal gain, reduce the threshold and play a positive role on the output power [12,19,20]. Simultaneously, the decreased area of ohmic contact also reduces the threshold current partly. The trenches will also suppress the lateral carrier leakage and hence improve the injection efficiency. In addition, the devices are bonded on the heatsink with p-side down, so the deep trenches and arrows reduce the thermal resistance, enhancing the heat dissipation and hence improving the power and PCE.

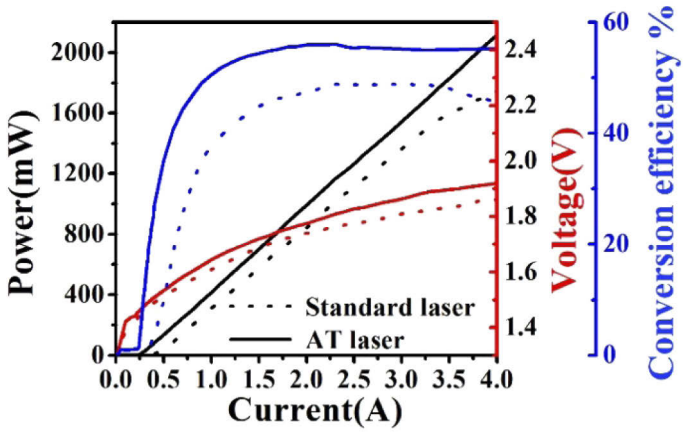

Fig. 5. CW L-I-V and conversion efficiency of standard lasers (dashed line) and AT lasers (solid lime) at 20 °C.

4.2. Far-field characteristics

Figure 6 shows the far-field profiles at 4 A for the AT laser and standard laser. The energy distribution of the lateral divergence is obviously improved. The profile of the AT laser is more concentrated, and the side lobes disappear as a result of the mode tailoring. The lateral divergences at 95% power content ($\theta_{L95\%}$) for the standard laser and AT laser are respectively 10.8° and 6.1°, corresponding to an improvement of 43.5%. The function of the microstructure is well represented, and these results also verify our simulation. The symmetric composite structure does suppress the high-order lateral modes, and the reduction of the lateral divergence is strong evidence of tailoring of the optical modes. Figure 7 shows the increase in the far-field angles as a function of injected current from 0.5 A to 4 A. The lateral divergence of the standard laser

Optics EXPRESS

increases from 3.4° to 10.8°, corresponding to an increasing rate of 2.1°/A. In contrast, the lateral divergence of the AT laser increases from 3.3° to 6.1°, so the increasing rate is 0.8°/A. The AT laser is less sensitive to the injection current, which means that far-field blooming is suppressed.

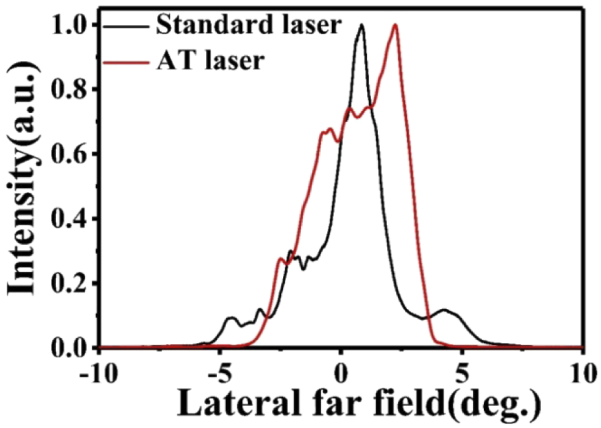

Fig. 6. Lateral far-field profiles of standard laser and AT laser at 4 A.

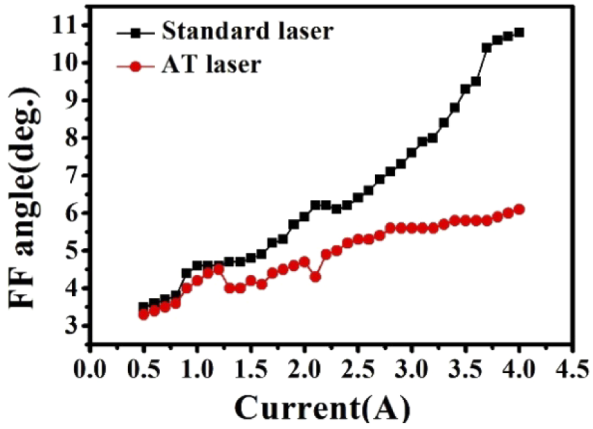

Fig. 7. Lateral divergence of the standard laser and AT laser depending on the injected current.

4.3. Near-field characteristics

Figure 8 shows the near-field profiles at 4 A. The near-field waists at 95% power ($w_{95\%}$) for these two structures are 128 μm for the standard laser and 94 μm for the AT laser. Figure 8 clearly shows that the profile of the AT laser is much narrower than that of the standard laser; the improvement is 26.5%. Figure 9 shows the dependence of the beam waist on the injected current. The beam waist of the standard BA laser increased rapidly and then became stable at approximately 125 μm. In contrast, the beam waist of the AT laser was narrower than that of the standard laser, decreasing from 116 μm to 94 μm as the current increased. The value of 94 μm is almost the same as the size of the injection window of the AT laser (~90 μm). These results may be attributed to the compression of the beam waist by the AT structure and the thermal lens effect. The former has been characterized in Figs. 2 and 3. The AT microstructure is able to supply strong support

Optics EXPRESS

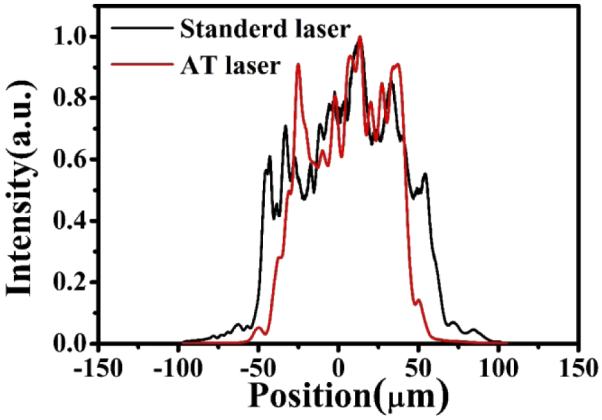

Fig. 8. Measured near-field profiles of the standard laser and AT laser at 4 A.

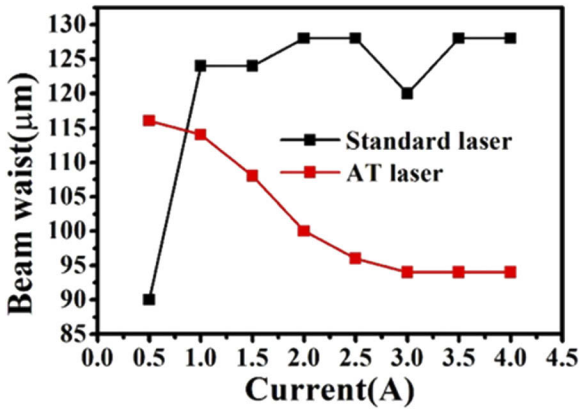

Fig. 9. Near-field waist of standard laser and AT laser depending on the injected current.

for a smaller beam waist; however, it is hard to give a reasonable explanation of the decreased beam waist with increasing injected current. This result can be attributed to the thermal lens effect. The thermal lens effect occurs because the local refractive index in the active region and waveguide of semiconductor lasers is affected by heat generated from the injection of carriers [21]. Temperature gradients arising from diffusion of heat induce a modulation of the refractive index distribution and contribute to the formation of a positive lens in the lateral dimension of the active area [22], corresponding to the increased refractive-index in the active region. Figure 10 shows the calculated distribution of the optical field of BA lasers, considering the thermal lens effect. The beam waists of the modes shrink when the refractive-index difference between the center and the edge of the BA ridge waveguide increases, which allows more high-order mode profiles to match the profile of the injected current. Subsequently, the new high-order modes arise on both sides of the BA waveguide and are tailored by the AT structure. Hence, at high injection current, the thermal lens effect tends to narrow the slow-axis near-field and may have a positive effect on the beam quality of the AT laser. As for the standard laser, the beam waist of high-order modes should also shrink because of the thermal lens effect. The intrinsic reason behind this result was found to be that the thermal lens effect will also result in the increasing order of lateral lasing modes [21], and each current step turns on an additional mode of higher order. Simultaneously, the fundamental mode is weakened by the increasing mode competition

Optics EXPRESS

and LCA, which provides more gain to higher-order modes [21,23]. Hence, the rising order of lateral lasing modes in the standard BA laser covers up the effect of near-field narrowing. Finally, the beam quality deteriorates when the current increases. Hence, the decreased beam waist of AT lasers shown in Fig. 9 should be a result of the combined effect of mode control by the AT microstructure and the thermal lens effect.

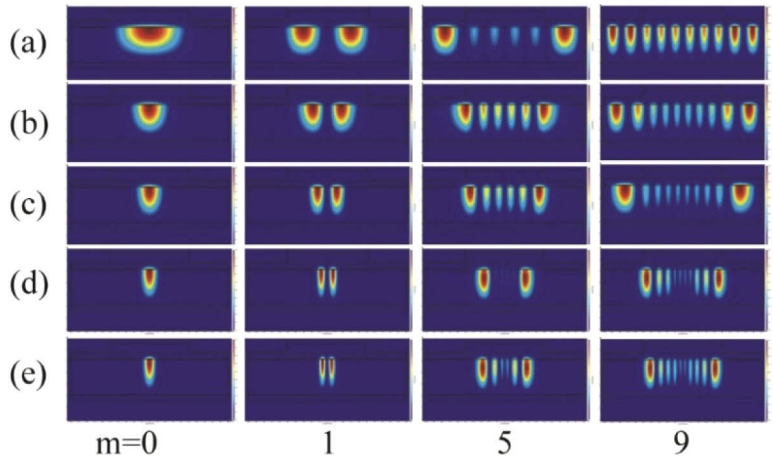

Fig. 10. The calculated near-field of BA laser for lateral mode orders of 0, 1, 5 and 9 when considering the thermal lens effect; (a)-(e) represent the refractive index difference between the center and the edge of the BA ridge waveguide as 0, 3×10^{-4}, 6×10^{-4}, 9×10^{-4} and 1.2×10^{-3}, respectively.

4.4. Lateral beam quality

The final lateral beam quality $BPP_{lat95\%}$ based on the above results is shown in Fig. 11, which shows that the BPP values of the standard laser and the AT laser are respectively 6.0 mm × mrad and 2.5 mm × mrad at 4 A, which means that the lateral beam quality is improved. The BPP value of the AT laser is much more stable than that of the standard laser; the improvement is 58% at 4 A. The dependence of the lateral BPP on the injection current for the standard laser

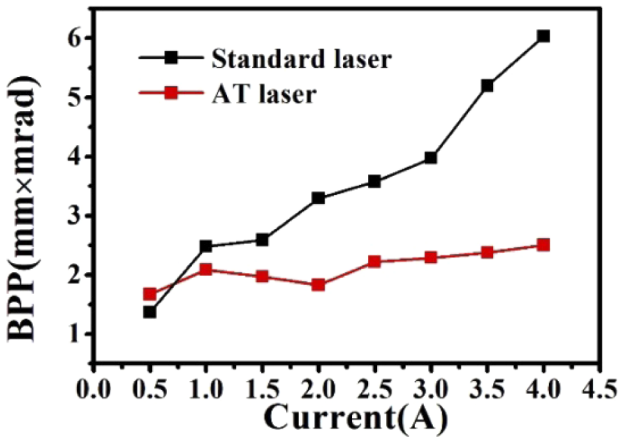

Fig. 11. Dependence of BPP values on current, measured from 0.5 A to 4 A.

Optics EXPRESS

is 1.33 mm × mrad /A, and this value is 0.23 mm × mrad/A for the AT laser. Obviously, the sensitivity of the BPP of the AT laser on the injection current improved significantly because of the shrinkage of the beam waist and the reduction of the lateral divergence. The corresponding improvement in lateral brightness was approximately 66%, which is extremely meaningful. To avoid the measurement error, multiple samples were tested. Table 1 shows more details about the two types of device. SL represents the standard laser. The absolute value of difference between the AT laser and standard laser is not same in the same batch and same wafer, but the general trend is that the beam quality and power performance of the AT laser are better than those of standard laser.

Table 1. Measured Performance of GaAs-based QW BALs

Sample number	Power (4 A)	PCE (max)	BPP (4 A)
SL 1	1.743 W	48.5%	6.0 mm × mrad
SL 2	1.679 W	47.7%	7.1 mm × mrad
SL 3	1.825 W	50.6%	7.2 mm × mrad
AT 1	2.117 W	55.2%	2.5 mm × mrad
AT 2	2.209 W	55.9%	2.9 mm × mrad
AT 3	2.250 W	56.8%	3.3 mm × mrad

5. Conclusion

In summary, we have demonstrated a new approach to improve the lateral beam quality via a composite arrow and trench microstructure, which can suppress the high-order lateral modes and lead to beam waist shrinkage, even at high injected current, together with the positive role of the thermal lens effect. Beam waist shrinkage and decreased far-field divergence with high output power were realized. The 58% improvement in $BPP_{lat95\%}$, 43.5% improvement in far-field lateral divergence, 26.5% improvement in beam waist, and 66% improvement in lateral brightness were achieved for 95% power content. We believe that these results will contribute to the development of high-power, high-brightness BA diode lasers.

Funding

Jilin Provincial Foundation (20180519024JH, 20190302053GX); National Natural Science Foundation of China (61761136009, 61774153).

Disclosures

The authors declare no conflicts of interest.

References

1. U. Witte, F. Schneider, M. Traub, D. Hoffmann, S. Drovs, T. Brand, and A. Unger, "kW-class direct diode laser for sheet metal cutting based on DWDM of pump modules by use of ultra-steep dielectric filters," Opt. Express **24**(20), 22917–22929 (2016).
2. A. Pietrzak, M. Zorn, R. Huelsewede, J. Meusel, and J. Sebastian, "Development of highly efficient laser diodes emitting around 1060nm for medical and industrial applications," Proc. SPIE **10900**, 109000K (2019).
3. N. Shimada, M. Yukawa, K. Shibata, K. Ono, T. Yagi, and A. Shima, "640-nm laser diode for small laser display," Proc. SPIE **7198**, 719806 (2009).
4. S. Hakobyan, V. Wittwer, P. Brochard, K. Gürel, S. Schilt, A. Mayer, U. Keller, and T. Südmeyer, "Fully-Stabilized Optical Frequency Comb from a Diode-Pumped Solid-State Laser with GHz Repetition Rate," in *Conference on Lasers and Electro-Optics, OSA Technical Digest (online)* (Optical Society of America, 2017), paper SF1C.1.
5. C. X. Yu, O. Shatrovoy, T. Y. Fan, and T. F. Taunay, "Diode-pumped narrow linewidth multi-kilowatt metalized Yb fiber amplifier," Opt. Lett. **41**(22), 5202–5205 (2016).

Optics EXPRESS

6. J. Piprek and Z. S. Li, "On the importance of non-thermal far-field blooming in broad-area high-power laser diodes," Appl. Phys. Lett. **102**(22), 221110 (2013).
7. K. Shigihara, Y. Nagai, S. Kakimoto, and K. Ikeda, "Achieving broad-area laser diodes with high output power and single-lobed far-field patterns in the lateral direction by loading a modal reflector," IEEE J. Quantum Electron. **30**(8), 1683–1690 (1994).
8. H. Wenzel, P. Crump, J. Fricke, P. Ressel, and G. Erbert, "Suppression of higher-order lateral modes in broad-area diode lasers by resonant anti-guiding," IEEE J. Quantum Electron. **49**(12), 1102–1108 (2013).
9. J. P. Hohimer, D. C. Craft, G. A. Vawter, and D. R. Myers, "Near-diffraction-limited angle-switchable output beam from a broad-area diode laser with an intracavity spatial phase controller," Appl. Phys. Lett. **58**(25), 2886–2888 (1991).
10. H. C. Eckstein, U. Zeitner, A. Tünnermann, C. Lauer, and U. Strauß, "Numerical simulation and optimization of microstructured high brightness broad area laser diodes," Proc. SPIE **9382**, 93821H (2015).
11. J. M. Rong, E. B. Xing, Y. Zhang, L. J. Wang, S. L. Shu, S. C. Tian, C. Z. Tong, X. L. Chai, Y. Q. Xu, H. Q. Ni, Z. C. Niu, and L. J. Wang, "Low lateral divergence 2 μm InGaSb/AlGaAsSb broad-area quantum well lasers," Opt. Express **24**(7), 7246–7252 (2016).
12. J. M. Rong, E. B. Xing, L. J. Wang, S. L. Shu, S. C. Tian, C. Z. Tong, and L. J. Wang, "Control of lateral divergence in high-power, broad-area photonic crystal lasers," Appl. Phys. Express **9**(7), 072104 (2016).
13. C. H. Tsai, Y. S. Su, C. W. Tsai, D. P. Tsai, and C. F. Lin, "High-power angled broad-area 1.3-(m laser diodes with good beam quality," IEEE Photonics Technol. Lett. **16**(11), 2412–2414 (2004).
14. M. Winterfeldt, P. Crump, S. Knigge, A. Maaßdorf, U. Zeimer, and G. Erbert, "High beam quality in broad area lasers via suppression of lateral carrier accumulation," IEEE Photonics Technol. Lett. **27**(17), 1809–1812 (2015).
15. T. Wang, C. Z. Tong, L. J. Wang, Y. G. Zeng, S. C. Tian, S. L. Shu, J. Zhang, and L. J. Wang, "Injection-insensitive lateral divergence in broad-area diode lasers achieved by spatial current modulation," Appl. Phys. Express **9**(11), 112102 (2016).
16. T. Wang, L. J. Wang, S. L. Shu, S. C. Tian, Z. D. Zhao, C. Z. Tong, and L. J. Wang, "Suppression of far-field blooming in high-power broad-area diode lasers by optimizing gain distribution," Chin. Opt. Lett. **15**(7), 071404 (2017).
17. Z. F. Lu, L. J. Wang, Y. Zhang, S. L. Shu, S. C. Tian, C. Z. Tong, G. Y. Hou, X. L. Chai, Y. Q. Xu, H. Q. Ni, Z. C. Niu, and L. J. Wang, "High-power GaSb-based microstripe broad-area lasers," Appl. Phys. Express **11**(3), 032702 (2018).
18. L. J. Wang, C. Z. Tong, S. L. Shu, S. C. Tian, F. Y. Sun, Y. Zhao, H. Y. Lu, X. Zhang, G. Y. Hou, and L. J. Wang, "Loss tailoring of high-power broad-area diode lasers," Opt. Lett. **44**(14), 3562–3565 (2019).
19. P. Crump, P. Leisher, T. Matson, V. Anderson, D. Schulte, J. Bell, J. Farmer, M. DeVito, R. Martinsen, Y. K. Kim, K. D. Choquette, G. Erbert, and G. Tränkle, "Control of optical mode distribution through etched microstructures for improved broad area laser performance," Appl. Phys. Lett. **92**(13), 131113 (2008).
20. A. F. Jonathan, A. B. Mikhail, and C. Federico, "Wide-ridge metal-metal terahertz quantum cascade lasers with high-order lateral mode suppression," Appl. Phys. Lett. **92**(3), 031106 (2008).
21. J. Piprek, "Inverse thermal lens effects on the far-field blooming of broad area laser diodes," IEEE Photonics Technol. Lett. **25**(10), 958–960 (2013).
22. H. An, Y. Xiong, C.-L. Jiang, B. Schmidt, and G. Treusch, "Methods for slow axis beam quality improvement of high power broad area diode lasers," Proc. SPIE **8965**, 89650U (2014).
23. J. Piprek, "Self-consistent far-field blooming analysis for high-power Fabry-Perot laser diodes," Proc. SPIE **8619**, 861910 (2013).